Pushing the envelope: force balance in fission yeast closed mitosis

Marcus A Begley[1], Christian Pagán Medina[1], Parsa Zareiesfandabadi[1,2], Matthew B Rapp[1], Mary Williard Elting[1,3*]

[1]Department of Physics, North Carolina State University, Raleigh, NC, [2]Present address: Department of Biology, Duke University, Durham, NC, [3]Quantitative and Computational Developmental Biology Cluster, North Carolina State University, Raleigh, NC

Correspondence: mary.elting@ncsu.edu

SUMMARY

The fission yeast *S. pombe* divides via closed mitosis. In short, mitotic spindle elongation and chromosome segregation transpire entirely within the complete nuclear envelope. Both the spindle and nuclear envelope must undergo significant conformation changes and are subject to varying external forces during this process. While the mechanical relationship between the two mitotic structures has been explored previously[1–4], much is still left to be discovered. Here, we investigate this relationship by observing the behaviors of spindles and nuclei in live mitotic fission yeasts following laser ablation. First, we characterize these dynamics in molecularly typical *S. pombe* spindles, finding them to be stabilized by dense crosslinking, before demonstrating that the compressive force acting on the spindle poles is higher in mitotic cells with greater nuclear envelope tension and that spindle compression can be relieved by lessening nuclear envelope tension. We finally examine the differences between the mitotic apparatus in *S. pombe* and *S. japonicus*, an evolutionary relative of *S. pombe* that undergoes semi-open mitosis, and show that *S. japonicus* mitotic spindles appear to both splay and bend more easily than those of their *S. pombe* relatives. Altogether, these data suggest that fission yeast spindle crosslinking may be tuned to support spindle extension and oppose nuclear envelope tension.

RESULTS AND DISCUSSION

S. pombe mitotic spindles are highly crosslinked

The *Schizosaccharomyces pombe* mitotic spindle consists of a single bundle of 10-20 microtubules, held together along its length by microtubule-crosslinking proteins[5–7]. In the spindle midzone, microtubules of alternating geometric polarity form a square lattice[5]. During anaphase, motor proteins can crosslink and slide apart antiparallel microtubule neighbors, creating extensile force within the spindle and driving spindle elongation[6,8]. In *S. pombe*, this elongation is quite dramatic with spindles elongating from hundreds of nanometers in length to roughly 10 μm over the course of mitosis[9,10]. Furthermore, these spindles are quite

spatiotemporally stereotyped, adhering to a strict protocol throughout mitosis[11], suggesting that fission yeasts can precisely tune their mitotic forces. The simplicity and standardization of the *S. pombe* mitotic apparatus allows us to effectively probe the fundamental physical characteristics of microtubule bundles subjected to different molecular perturbations.

We began by characterizing spindle structure in control *S. pombe* cells using laser ablation of live cells[12] (Figure 1A). Upon ablation, the two spindle halves collapse toward each other in a motor driven process, bringing the two poles together and reforming the spindle[8,12,13] (Figure 1A). Before a spindle reforms, the two half-spindles are detached from each other, and microtubules within each half bundle can either stay tightly associated with each other or become detached along their lengths, a process that we term “splaying”[14].

Comparison of the probability of each of these two behaviors creates an indicator of the degree of crosslinking between the microtubules in the ablated spindle[14]. In *S. pombe*, ablated spindle halves splay only rarely (Figure 1B), suggesting a high degree of crosslinking, consistent with previous work characterizing *S. pombe* spindle structure. Another striking feature of the behavior of *S. pombe* spindle halves following severing by laser ablation is that their overall length is maintained, with very little shortening (Figure 1A, C). We expect the spindle at the point of severing (generally near the center of the spindle) to form an antiparallel architecture[5], and thus for approximately half of the microtubule ends in each bundle created by laser ablation to have their plus-ends facing toward the site of ablation. A typical hallmark of the response to laser ablation of microtubules in many cell types is depolymerization of “naked” plus-ends created by microtubule severing[15–18]. Thus, it was initially surprising to us that such behavior is so rarely observed in these spindles (Figure 1A, C). High densities of crosslinking proteins have been shown to stabilize microtubule bundles against catastrophic depolymerization[19,20]. Therefore, the fact that spindle halves mostly resist depolymerization following ablation provides additional evidence that *S. pombe* spindles are highly crosslinked. Indeed, such crosslinking is also consistent with the highly stereotyped organization of the central spindle at this stage[5]. Altogether, these data paint a picture of the *S. pombe* mitotic spindle as a tightly-bound microtubule bundle that is stable, even under significant physical disturbance.

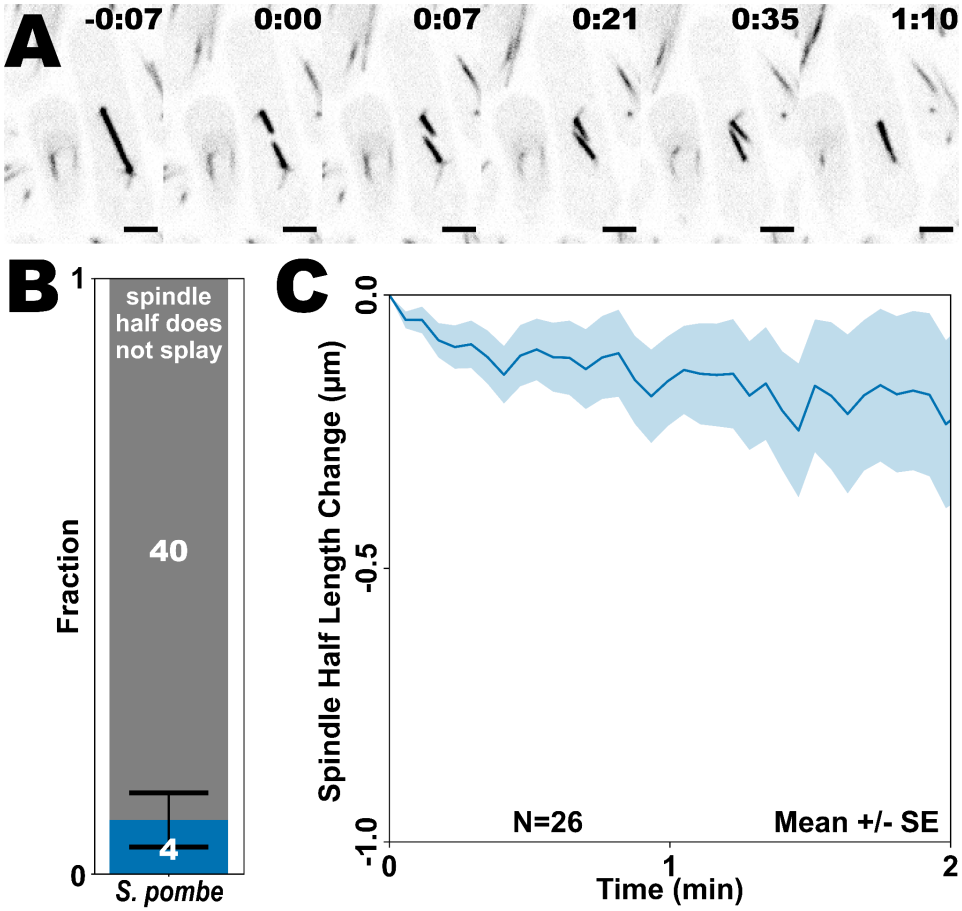

Figure 1: *S. pombe* mitotic spindles are highly crosslinked. (A) Typical example of laser ablation of an *S. pombe* spindle expressing GFP-Atb2 (MWE2), showing post-ablation spindle collapse, followed by the reattachment of ablated spindle halves at their plus-ends. Scale bars are 2 µm and timestamps are in min:sec. (B) Ablated *S. pombe* spindle halves rarely splay apart. Error bar indicates the square root of the number of splayed events, as an estimate on the variation in this number assuming Poisson statistics. (C) *S. pombe* spindles do not depolymerize much, following ablation. The y-axis is the change in spindle half length, compared to the first frame after ablation. The line represents the average spindle half length change and the shaded region represents average +/- standard error on the mean.

Ase1 crosslinking prevents microtubule depolymerization in *S. pombe*

An important component of the *S. pombe* mitotic spindle is the passive microtubule-microtubule crosslinking protein Ase1, which preferentially localizes to antiparallel microtubule overlaps in the spindle midzone, particularly at anaphase[10,21–23]. Here, it functions to stabilize the spindle midzone and is therefore implicated in the modulation of spindle dynamics. Namely, Ase1 supports bipolar spindle formation in *S. pombe* through its stabilization of microtubule bundles, and even allows the formation of a bipolar spindle in the absence of kinesin-5 mediated antiparallel microtubule sliding[24]. Intriguingly, Ase1 has also been shown, through the same

underlying mechanism of antiparallel microtubule stabilization, to slow motor-driven anaphase spindle elongation in budding yeast[7,25]. Thus, we sought to investigate the role of Ase1 in the highly crosslinked nature of *S. pombe* spindles.

To this end, we laser ablated mitotic spindles in Ase1-deletion (*ase1Δ*) *S. pombe*, similar to the experiments described above in cells with normal Ase1 expression. Strikingly, rapid ablated spindle half depolymerization was common in *ase1Δ* cells (Figure 3), consistent with the role of Ase1 in stabilizing bundles[19,24,25]. Though this depolymerization prevented reliable characterization of post-ablation spindle half splaying as for control *S. pombe* cells (Figure 1), some splaying was visible of the remaining spindle halves as they depolymerized (Figure 2A). These data are consistent overall with a central role for Ase1 in both crosslinking *S. pombe* spindles and stabilizing their microtubules.

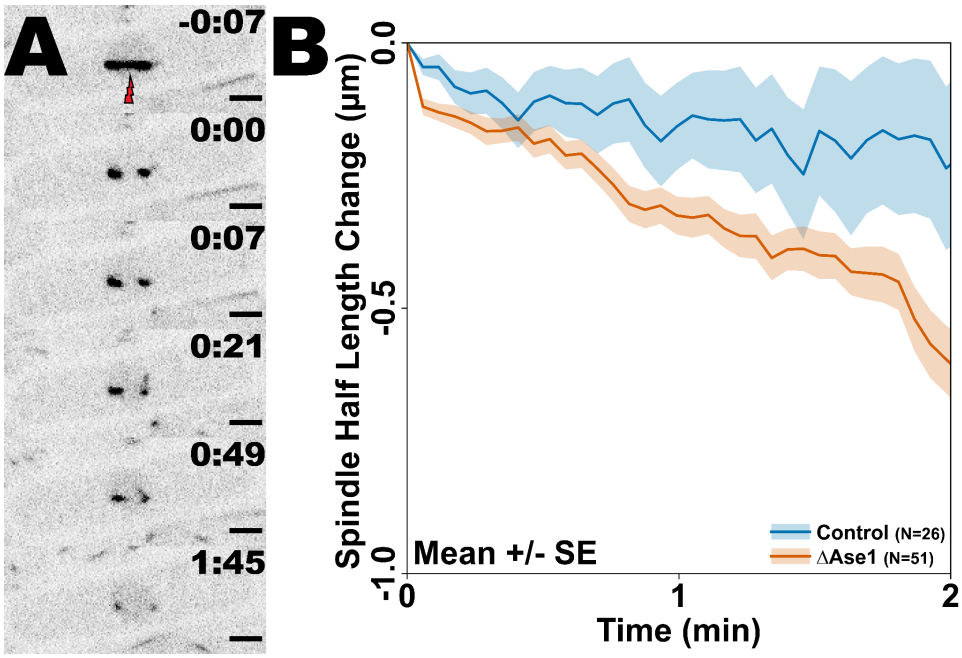

Figure 2: Ase1 crosslinking prevents microtubule depolymerization in *S. pombe*. (A) Typical example of spindle ablation in *ase1Δ S. pombe* expressing GFP-Atb2 (MWE3), in which both spindle halves depolymerize. Some spindle splaying is also visible during depolymerization (0:49). Scale bars are 2 µm and timestamps are in min:sec. (B) *ase1Δ S. pombe* (orange) halves tend to depolymerize more quickly and severely than those from *S. pombe* with unperturbed ase1 (blue, same data as Figure 1C), as shown by traces of the average change in spindle half length after ablation. Traces represent averages across all videos and shaded regions represent average +/- standard error on the mean.

The fission yeast spindle and nuclear envelope are a mechanical pair

While the *S. pombe* anaphase spindle elongates, the nuclear envelope undergoes drastic conformational changes, beginning as a spheroid before transitioning into a dumbbell-like shape[1,3]. Simultaneously, the spindle elongates, but still remains an approximately linear bundle[1]. The spindle and nuclear envelope are mechanically linked at the two spindle pole

bodies (SPBs), which nest into the nuclear envelope during mitosis in *S. pombe*[26]. To probe the mechanical effect that nuclear envelope tension has on the spindle, we performed laser ablations in cerulenin-treated *S. pombe* (Figure 3). Cerulenin is a fatty acid synthesis inhibitor that prevents the addition of phospholipids to the nuclear envelope during nuclear envelope expansion, and has previously been shown to alter *S. pombe* mitotic nuclear shape[1,27]. In *S. pombe*, cerulenin-treatment has been shown to greatly increase nuclear envelope tension, which in turn can often lead to bending in anaphase spindles[1] (Figure 3A and B). We performed two sets of laser ablation experiments in cerulenin-treated cells.

First, we selectively ablated mitotic spindles that appear curved, presumably due to the increased surface tension causing the spindle to bow or bend (Figure 3A). Consistent with this interpretation, the two spindle fragments straighten upon ablation. After severance, the incident angle between the two halves is much greater than that of straight spindles. As with spindles in control *S. pombe*, the two spindle poles collapse toward each other after ablation in cerulenin-treated cells, however at a much greater rate (Figure 3C). Because the misaligned configuration of the two ablated fragments would not be conducive to motor transport, compared to the aligned conformation of ablated control spindles (Figure 1A), this suggests an increase in compressive force acting on the spindle ends from the stretched nuclear envelope. Interestingly, these spindles rarely repair and, after failing to reconnect, ablated spindle halves often appear to depolymerize (Figure 3A, left spindle half).

Secondly, we perform experiments in which we ablate the nuclear envelope of cerulenin-treated *S. pombe* and track the changes to the spindle and nucleoplasm (Figure 3B). This experiment allows us to test whether the envelope tension is indeed the direct mechanical cause of spindle bending. For these experiments, we use cells expressing both GFP-Atb2 (to visualize tubulin) and GFP-NLS, which enables us to determine whether we successfully open the nuclear envelope, allowing nucleoplasm to leak into the cytoplasm. Here, we also observe a viscoelastic-like ablation response of the spindle. Usually within a minute following ablation, the spindle straightens from a curved conformation to its relaxed, straight state (Figure 3B, D). This implies a reduction in the compressive force acting on the spindle poles and provides additional evidence of nuclear envelope tension as the source of this force. Furthermore, we typically observe spindle relaxation in concurrence with nucleoplasm leakage, visualized by the weakening intensity of GFP-NLS signal in the nucleus (Figure 3B). This correlation is apparent through the nearly overlapping curves of average spindle curvature and average nuclear (GFP-NLS) intensity over time, following ablation (Figure 3D). Note the delay, at the individual cell level, following many of the nuclear envelope ablations before substantial spindle and nuclear envelope relaxation (Figure 3E, inset). The duration of these two delays in spindle collapse and in nucleoplasm leakage onset are highly correlated, suggesting a causative relationship (Figure 3E). Because both the spindle and nuclear envelope tend to relax nearly simultaneously, we hypothesize that the initial nuclear envelope ablation, while likely small in area, triggers a subsequent catastrophic event in which the hole expands and nuclear envelope tension plummets.

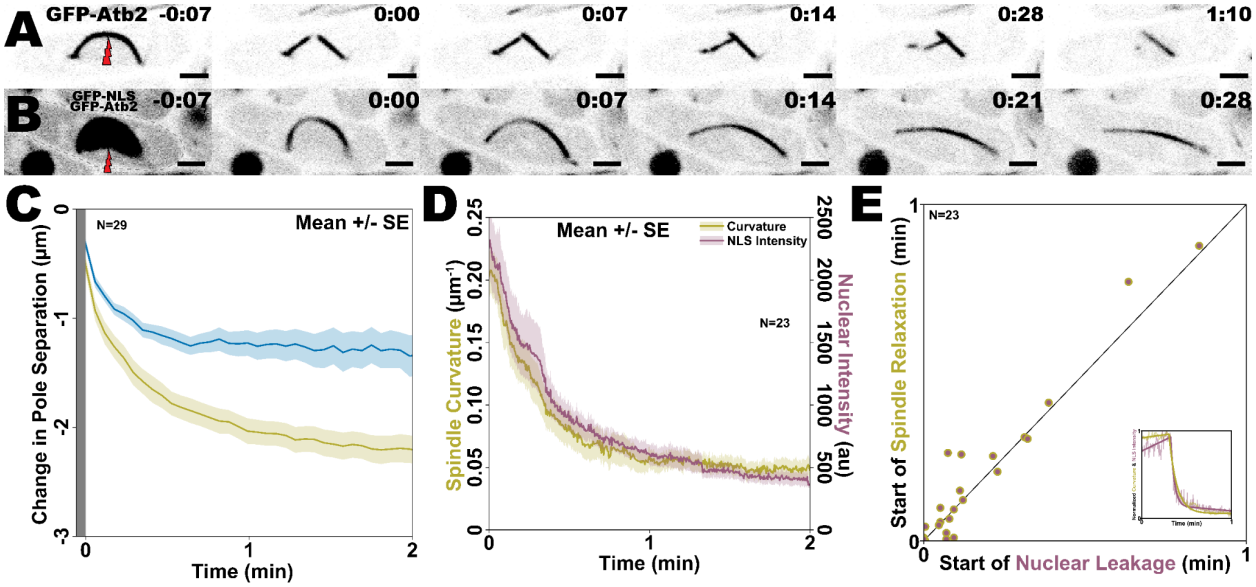

Figure 3: The fission yeast spindle and nuclear envelope are a mechanical pair. (A) Typical example of spindle ablation in cerulenin-treated *S. pombe* cell expressing GFP-Atb2 (MWE2). Dynamic changes to spindle structure seen here include spindle half straightening (0:00), spindle collapse, and unrepaired spindle half depolymerization (left half, 1:10). Scale bars are 2 μm and timestamps are in min:sec. (B) Typical example of nuclear envelope ablation in cerulenin-treated *S. pombe* cell expressing GFP-Atb2 and GFP-NLS (MWE48), showing nucleoplasm leakage and spindle relaxation, following nuclear envelope rupture. Scale bars are 2 μm and timestamps are in min:sec. (C) Cerulenin-treated *S. pombe* spindles (gold) collapse much faster and more severely than spindles in untreated *S. pombe* (blue). All cells strain MWE2. Traces represent average change in pole separation, compared to the first frame after ablation, and shaded regions represent average +/- standard error on the mean. (D) The averages of NLS intensity (purple) and spindle curvature (gold) show similar trajectories, following ablation. Traces represent averages across all videos and shaded regions represent average +/- standard error on the mean. All cells strain MWE48. (E) The initiations of nucleoplasm leakage and spindle relaxation, defined using best fit traces for each individual video, are approximately simultaneous. (E - inset) Example of typical NLS intensity (purple) and spindle curvature (gold) traces, following laser ablation of cerulenin-treated *S. pombe* nuclear envelopes. Jagged traces represent raw data and smooth lines show fits to the raw data, which have been normalized to the highest NLS intensity and spindle curvature values for that video.

S. japonicus spindles are less crosslinked than the *S. pombe* spindles and do not have to oppose as much compressive force

We next took a comparative biology approach to examine how the trends we observed in *S. pombe* compared to the fission yeast *Schizosaccharomyces japonicus*. In general, the *S. japonicus* and *S. pombe* mitotic machinery share many commonalities. The spindle forms a spindle microtubule bundle as it elongates throughout anaphase and spindle elongation accompanies significant changes in nuclear envelope shape. However, there are notable

differences between the two systems that are especially relevant to our study. Importantly, unlike in *S. pombe*, which maintains nuclear envelope closure throughout its lifecycle, partial nuclear envelope breakdown can occur during chromosome segregation in *S. japonicus*, in a process known as semi-open mitosis[1,28,29]. Because the nuclear envelope is incomplete for much of anaphase, the mitotic spindle in *S. japonicus* elongates while experiencing a lower level of nuclear envelope tension than in *S. pombe*.

Mitotic spindles of the two fission yeasts, like their nuclear envelopes, look generally similar at the beginning and end of anaphase, but can diverge in their intermediate conformations. Notably, the *S. pombe* spindle appears quite straight throughout mitosis, whereas *S. japonicus* spindles often bend, especially in late anaphase[1]. This suggests a possible divergence in spindle structure between the two evolutionary cousins. To explore possible effects on the mechanical relationship between the spindle and nuclear envelope in these two yeasts, we repeated many of the experiments described above in *S. japonicus*.

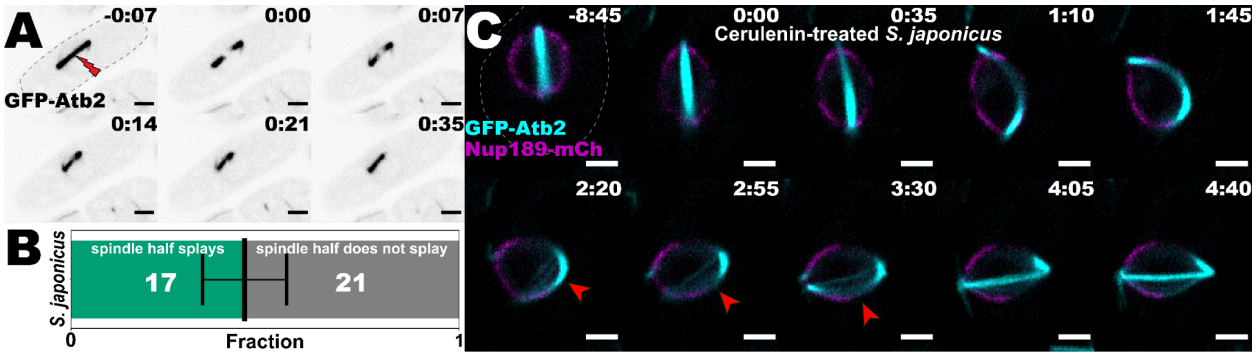

Figure 4: *S. japonicus* spindles are less crosslinked than *S. pombe* spindles and do not have to oppose as much compressive force. (A) Typical example of spindle ablation in *S. japonicus* cell expressing GFP-Atb2 (strain MWE92, Nup189-mCherry expressed but not imaged), showing the splaying apart of microtubules at the plus ends of one of the ablated spindle halves (upper right), but not the other (lower left). Scale bars are 2 μm and timestamps are in min:sec. (B) Nearly half of ablated *S. japonicus* spindle halves splay apart at some point during spindle repair (compare to Figure 1B). Error bar indicates the square root of the number of splayed events, as an estimate on the variation in this number assuming Poisson statistics. (C) Rare example of cerulenin-treated *S. japonicus* cell expressing GFP-Atb2 and Nup189-mCherry (strain MWE92) showed extreme bending, with some individual microtubules mechanically dissociating with the rest of the bundle as it bows excessively (2:20-3:30).

First, we laser ablated anaphase *S. japonicus* spindles and investigated the frequency with which the microtubules in spindle halves splay apart following laser ablation (Figure 4A). Strikingly, while splaying was rare in *S. pombe* ablated spindle halves (Figure 1B), the plus-ends of at least some microtubules mechanically dissociated in nearly half of all ablated *S. japonicus* spindle halves (Figure 4A, B), suggesting that microtubules in these spindles are less tightly-bound to each other along their lengths than their *S. pombe* counterparts. Further evidence that *S. japonicus* spindles may be less cohesive than *S. pombe* spindles comes from observations of mitotic progression in cerulenin-treated cells. Here, cerulenin-treated *S. japonicus* are imaged, without mechanical perturbations such as laser ablation, as spindles

attempt anaphase elongation. Rarely, but strikingly, we see constrained spindles bow, as they elongate inside a more tense nuclear envelope (Figure 4C). We never observe such dramatic bending in *S. pombe*, and their ability to undergo such bending suggests that *S. japonicus* spindles may be less rigid than *S. pombe* spindles. Additionally, as the spindle shown in Figure 4C bends, individual microtubules appear to dissociate with the rest of the spindle in its midsection, while remaining bound at the centrosomes (red arrow), a behavior that we never observe in *S. pombe* spindles. This behavior suggests a possible mechanism for the apparently decreased rigidity of *S. japonicus* spindles: they may either be less densely or robustly crosslinked, allowing microtubules to detach from the main spindle bundle when subjected to sufficient compressive force. While examples of extreme spindle bending are quite rare among cerulenin-treated *S. japonicus*, occurring in only two of the observed cells, this phenomenon was never observed in cerulenin-treated *S. pombe*. It is also important to note that, although this was only observed in two cells, we only found three curved spindles in all of our imaging of cerulenin-treated *S. japonicus*. We suppose that this lack of curved spindles is likely due to the frequency at which *S. japonicus* nuclear envelopes locally break down, thereby relieving nuclear envelope tension and allowing spindles to straighten, a noted difference between untreated *S. pombe* and *S. japonicus* cells[1].

In total, our results demonstrate significant mechanical coupling, during mitosis, between the mitotic spindle and nuclear envelope in fission yeasts. The rapid spindle collapse following spindle ablation in cerulenin-treated *S. pombe* suggests the presence of a compressive force on the spindle poles, resulting from increased nuclear envelope tension. Likewise, the simultaneous nuclear envelope rupture and spindle relaxation after nuclear envelope ablation implies this compressive force can be lessened by relieving tension in the nuclear envelope. The high degree of crosslinking in the *S. pombe* spindle likely allows it to oppose a typical level of nuclear envelope tension to remain straight during normal mitosis, when nuclear envelope expansion accommodates an elongating anaphase spindle. In contrast, *S. japonicus* spindles appear less crosslinked, since their microtubules more easily splay apart from the main bundle and the spindle as a whole bends more readily. These mechanical features are consistent with a lower need to oppose nuclear envelope tension in semi-open mitosis. While previous work has described differences in the nuclear envelopes of the two species during mitosis[1,30,31], little is known about the molecular-level structure and organization of the *S. japonicus* mitotic spindle. Future work could provide further insight into how the mechanical properties of these two functionally integrated structures, the mitotic spindle and the nuclear envelope, may have co-evolved to support robust chromosome segregation and genetic integrity.

Materials and Methods

RESOURCE AVAILABILITY

Lead contact

Further information and requests for resources and reagents should be directed to and will be fulfilled by the Lead Contact, Mary Williard Elting (mary.elting@ncsu.edu).

FISSION YEAST STRAINS AND CULTURE

All experiments were performed using cells from the two fission yeast species, *Schizosaccharomyces pombe* and *Schizosaccharomyces japonicus*. For strain details, see Key Resources table. *S. pombe* strains MWE2 and MWE3 are from Fred Chang lab stock (original strains FC2861 and FC1984[23], respectively). MWE48 was created by crossing *S. pombe* strains MWE2 and MWE40, which was from Gautam Dey lab stock (original strain GD208[32]). Cross was performed by tetrad dissection using standard methods[33]. *S. japonicus* strain MWE92 was from Snezhana Oliferenko lab stock (original strain SOJ398[1]). Both *S. pombe* and *S. japonicus* strains were cultured at 25C on YE5S plates using standard techniques[33]. For imaging, liquid cultures were grown in YE5S media at 25 °C with shaking by a rotating drum for 12-24 hours before imaging. To ensure that cells were in growth phase for imaging, we measured OD595 with a target of 0.1-0.2. If cells had grown beyond this point, we diluted them and allowed them to recover for ~1 hour before imaging.

As a method of increasing nuclear envelope tension in *S. pombe* and *S. japonicus,* cells were treated with 1mM cerulenin, from stock solutions at 50 mM in DMSO, as previously described[1,27].

LIVE CELL IMAGING AND LASER ABLATION

Spinning disk confocal live imaging and laser ablation experiments were performed similar to those described previously[9,12,14]. Live videos were captured using a Nikon Ti-E stand on an Andor Dragonfly spinning disk confocal fluorescence microscope; spinning disk dichroic Chroma ZT405/488/561/640rpc; 488 nm (50 mW) diode laser (240 ms exposures) with Borealis attachment (Andor); emission filter Chroma Chroma ET525/50m; and an Andor iXon3 camera. Imaging was performed with a 100x 1.45 Ph3 Nikon objective and a 1.5x magnifier (built-in to the Dragonfly system). An Andor Micropoint attachment with galvo-controlled steering was used for targeted laser ablation, delivering 20-30 3 ns pulses of 551 nm light at 20 Hz. Each cell was imaged until either spindle repair had been completed or the spindle had failed to repair after ~5 min. For spindle ablation videos frames were collected every 3.5 s, while frames were collected every 280 ms for nuclear envelope ablation videos. Andor Fusion software was used to manage imaging and Andor IQ software was used to simultaneously manipulate the laser ablation system.

Prior to imaging, samples were placed onto gelatin pads on microscope glass slides. For gelatin pads, 125 mg gelatin was added to 500 µL EMM5S and heated, in a tabletop dry heat bath at 90°C for at least 20 min. A small sample volume (~5 µL) of the gelatin mixture was pipetted onto each slide, covered with a coverslip, and given a minimum of 30 min to solidify. For each microscope slide, 1 mL volume of cells suspended in YE5S liquid growth media were centrifuged (enough to see a pellet), using a tabletop centrifuge. Nearly all the supernatant was decanted and the cells were resuspended in the remaining supernatant. Next, 2 µL of resuspended cells were pipetted onto the center of the gelatin pad, which was immediately covered with a cover slip. Finally, the coverslip is sealed using VALAP (1:1:1:

Vaseline:lanolin:paraffin). All samples, sealed between the gelatin pads and coverslips, were imaged at room temperature (~22°C).

QUANTIFICATION AND STATISTICAL ANALYSIS

Image and video preparation and editing

To optimize the identification and tracking of spindle and nuclear envelope features, modifications were made to fluorescence microscopy images and videos using FIJI[34]. First, images and videos were cropped to show only cells of interest and extra frames were eliminated. Typically, linear adjustments were made to the brightness and contrast of the images, in order to track features more clearly. For measurements of NLS intensity, however, pixel intensities were measured from unadjusted images. For immunofluorescence images, the same brightness and contrast scaling was used for all images in each set.

Tracking of spindle features in ablation videos

All quantitative data regarding post-ablation spindle dynamics was collected via a tracking program, home-written in Python. For each ablated spindle, the two spindle poles are tracked following ablation, using this program, and the 'line' tool in FIJI is used to measure the length of each spindle immediately prior to ablation. This data is then used to calculate the change in pole separation (length) for each spindle over time, following ablation. Additionally, the positions of the two new plus-ends of each ablated spindle half are tracked throughout the video. Our tracking program includes a method for indicating whether or not spindle repair has occurred, with the reconnection of the two ablated spindle halves, in each frame. The data for frames collected before the reformation of a single spindle is used to compute time traces for the change in spindle half length.

We define spindle half splaying as the lateral dissociation of microtubule ends from each other in ablated spindle halves. Splay state is determined by eye in FIJI, using videos in which the brightness and contrast have been linearly adjusted for clarity. If a spindle half appears splayed in any frame of a video, that spindle half is counted as splaying. Otherwise, it is counted as a spindle that does not splay. For videos in which splay state is not readily apparent throughout, for one or both spindle halves, no splaying designation is made for the unclear half/halves. In some cases, a spindle half depolymerizes within the first few minutes following ablation and is therefore not included in our splay state analysis.

Quantification of spindle relaxation and nucleoplasm leakage

For all nuclear envelope ablation videos, data was collected on the time-evolution of spindle curvature using a home-written Matlab program. The program takes microscope image files and fits a quadratic function to a chosen object in the image. It then outputs curvature and length data from that fitted curve. For videos this process was semi-automated to perform the fit frame-by-frame.

Another program, home-written in Python was used to track the rate of nucleoplasm leakage from the nucleus of each cell following nuclear envelope ablation. This program requires the unadjusted video, spindle curvature data, and spindle length data as inputs. Using these inputs, nuclear intensity is calculated for each frame as the average GFP intensity (after

background subtraction) of a 25-pixel square near the center of the nucleus. This same program is then used to compute best-fit curves for both post-ablation spindle curvature and nuclear intensity.

KEY RESOURCES TABLE

REAGENT of RESOURCE	SOURCE	IDENTIFIER
Chemicals, peptides, and other recombinant proteins		
Cerulenin	Genesee Scientific	Cat# J64538.#0
Experimental models: Organisms/strains		
S. pombe h+ GFP-atb2:kanMX ade6- leu1-32 ura4-D18	F. Chang (FC2861)	MWE2
S. pombe h? ase1::KanMX leu1-32::SV40-GFP-atb2[LEU1] leu1-32 ura4-D18 his7+	F. Chang (FC1984[23])	MWE3
S. pombe h- pBIP1-NLS-GFP-NLS:leu1+ ade-leu1-32 ura4D-18	G. Dey (GD208[32])	MWE40
S. pombe pBIP1-NLS-GFP-NLS:leu1+ GFP-atb2:kanMX	This work (cross of MWE2 and MWE40)	MWE48
S. japonicus GFP-Atb::ura4+ Nup189-mCherry::ura4+ urasj-D3 ade6sj-domE	S.Oliferenko (SOJ398[1])	MWE92
Software and algorithms		
Jupyter Notebook	Project Jupyter	
MATLAB	MathWorks	
Fiji	ImageJ	

ACKNOWLEDGEMENTS

We thank M. Betterton, G. Dey, F. Chang, A. Molînes, S. Oliferenko, and members of the Elting lab for advice and helpful discussions, and we thank F. Chang, G. Dey, and S. Oliferenko for strains. We thank the Weninger Lab (NCSU) and Wang Lab (NCSU) for sharing lab space and equipment. We thank the Cellular and Molecular Imaging Facility (CMIF) at NCSU for microscopy support. This work was supported by NIH 1R35GM138083 and NSF 2133276.

REFERENCES

1. Yam, C., He, Y., Zhang, D., Chiam, K.-H., and Oliferenko, S. (2011). Divergent strategies for controlling the nuclear membrane satisfy geometric constraints during nuclear division. Curr. Biol. *21*, 1314–1319. 10.1016/j.cub.2011.06.052.

2. Mori, R., and Oliferenko, S. (2020). Cell Biology: An Open Solution for Closed Mitosis. Curr. Biol. *30*, R942–R944. 10.1016/j.cub.2020.06.067.

3. Zhu, Q., Zheng, F., Liu, A.P., Qian, J., Fu, C., and Lin, Y. (2016). Shape Transformation of the Nuclear Envelope during Closed Mitosis. Biophys. J. *111*, 2309–2316. 10.1016/j.bpj.2016.10.004.

4. Fang, C., Zheng, F., Yao, J., Wei, X., Fu, C., Shi, X., and Lin, Y. (2020). A model for bridging microtubule dynamics with nuclear envelope shape evolution during closed mitosis. J. Mech. Phys. Solids *144*, 104116. 10.1016/j.jmps.2020.104116.

5. Ding, R., McDonald, K.L., and McIntosh, J.R. (1993). Three-dimensional reconstruction and analysis of mitotic spindles from the yeast, Schizosaccharomyces pombe. Journal of Cell Biology *120*, 141–151. 10.1083/jcb.120.1.141.

6. Krüger, L.K., Gélin, M., Ji, L., Kikuti, C., Houdusse, A., Théry, M., Blanchoin, L., and Tran, P.T. (2021). Kinesin-6 Klp9 orchestrates spindle elongation by regulating microtubule sliding and growth. Elife *10*, e67489. 10.7554/eLife.67489.

7. Thomas, E.C., Ismael, A., and Moore, J.K. (2020). Ase1 domains dynamically slow anaphase spindle elongation and recruit Bim1 to the midzone. Mol. Biol. Cell *31*, 2733–2747. 10.1091/mbc.E20-07-0493-T.

8. Tolić-Nørrelykke, I.M., Sacconi, L., Thon, G., and Pavone, F.S. (2004). Positioning and elongation of the fission yeast spindle by microtubule-based pushing. Curr. Biol. *14*, 1181–1186. 10.1016/j.cub.2004.06.029.

9. Uzsoy, A.S.M., Zareiesfandabadi, P., Jennings, J., Kemper, A.F., and Elting, M.W. (2021). Automated tracking of S. pombe spindle elongation dynamics. J. Microsc. *284*, 83–94. 10.1111/jmi.13044.

10. Loïodice, I., Staub, J., Setty, T.G., Nguyen, N.-P.T., Paoletti, A., and Tran, P.T. (2005). Ase1p organizes antiparallel microtubule arrays during interphase and mitosis in fission yeast. Mol. Biol. Cell *16*, 1756–1768. 10.1091/mbc.E04-10-0899.

11. Nabeshima, K., Nakagawa, T., Straight, A.F., Murray, A., Chikashige, Y., Yamashita, Y.M., Hiraoka, Y., and Yanagida, M. (1998). Dynamics of Centromeres during Metaphase–Anaphase Transition in Fission Yeast: Dis1 Is Implicated in Force Balance in Metaphase Bipolar Spindle. MBoC *9*, 3211–3225. 10.1091/mbc.9.11.3211.

12. Zareiesfandabadi, P., and Elting, M.W. (2022). Force by minus-end motors Dhc1 and Klp2 collapses the S. pombe spindle after laser ablation. Biophys. J. *121*, 263–276. 10.1016/j.bpj.2021.12.019.

13. Khodjakov, A., La Terra, S., and Chang, F. (2004). Laser microsurgery in fission yeast; role

of the mitotic spindle midzone in anaphase B. Curr. Biol. *14*, 1330–1340. 10.1016/j.cub.2004.07.028.

14. Begley, M.A., Solon, A.L., Davis, E.M., Sherrill, M.G., Ohi, R., and Elting, M.W. (2021). K-fiber bundles in the mitotic spindle are mechanically reinforced by Kif15. Mol. Biol. Cell *32*, br11. 10.1091/mbc.E20-06-0426.

15. Maiato, H., Rieder, C.L., and Khodjakov, A. (2004). Kinetochore-driven formation of kinetochore fibers contributes to spindle assembly during animal mitosis. J. Cell Biol. *167*, 831–840. 10.1083/jcb.200407090.

16. Spurck, T.P., Stonington, O.G., Snyder, J. a., Pickett-Heaps, J.D., Bajer, A., and Mole-Bajer, J. (1990). UV microbeam irradiations of the mitotic spindle. II. Spindle fiber dynamics and force production. J. Cell Biol. *111*, 1505–1518.

17. Brugués, J., Nuzzo, V., Mazur, E., and Needleman, D.J. (2012). Nucleation and transport organize microtubules in metaphase spindles. Cell *149*, 554–564. 10.1016/j.cell.2012.03.027.

18. Sheykhani, R., Baker, N., Gomez-Godinez, V., Liaw, L.-H., Shah, J., Berns, M.W., and Forer, A. (2013). The role of actin and myosin in PtK2 spindle length changes induced by laser microbeam irradiations across the spindle. Cytoskeleton *70*, 241–259. 10.1002/cm.21104.

19. Stoppin-Mellet, V., Fache, V., Portran, D., Martiel, J.-L., and Vantard, M. (2013). MAP65 coordinate microtubule growth during bundle formation. PLoS One *8*, e56808. 10.1371/journal.pone.0056808.

20. Ichihara, K., Kitazawa, H., Iguchi, Y., Hotani, H., and Itoh, T.J. (2001). Visualization of the stop of microtubule depolymerization that occurs at the high-density region of microtubule-associated protein 2 (MAP2). J. Mol. Biol. *312*, 107–118. 10.1006/jmbi.2001.4934.

21. Janson, M.E., Loughlin, R., Loïodice, I., Fu, C., Brunner, D., Nédélec, F.J., and Tran, P.T. (2007). Crosslinkers and motors organize dynamic microtubules to form stable bipolar arrays in fission yeast. Cell *128*, 357–368. 10.1016/j.cell.2006.12.030.

22. Yamashita, A., Sato, M., Fujita, A., Yamamoto, M., and Toda, T. (2005). The roles of fission yeast ase1 in mitotic cell division, meiotic nuclear oscillation, and cytokinesis checkpoint signaling. Mol. Biol. Cell *16*, 1378–1395. 10.1091/mbc.E04-10-0859.

23. Bratman, S.V., and Chang, F. (2007). Stabilization of overlapping microtubules by fission yeast CLASP. Dev. Cell *13*, 812–827. 10.1016/j.devcel.2007.10.015.

24. Rincon, S.A., Lamson, A., Blackwell, R., Syrovatkina, V., Fraisier, V., Paoletti, A., Betterton, M.D., and Tran, P.T. (2017). Kinesin-5-independent mitotic spindle assembly requires the antiparallel microtubule crosslinker Ase1 in fission yeast. Nat. Commun. *8*, 15286. 10.1038/ncomms15286.

25. Braun, M., Lansky, Z., Fink, G., Ruhnow, F., Diez, S., and Janson, M.E. (2011). Adaptive braking by Ase1 prevents overlapping microtubules from sliding completely apart. Nat. Cell Biol. *13*, 1259–1264. 10.1038/ncb2323.

26. Ding, R., West, R.R., Morphew, D.M., Oakley, B.R., and McIntosh, J.R. (1997). The spindle pole body of Schizosaccharomyces pombe enters and leaves the nuclear envelope as the cell cycle proceeds. Mol. Biol. Cell *8*, 1461–1479. 10.1091/mbc.8.8.1461.

27. Awaya, J., Ohno, T., Ohno, H., and Omura, S. (1975). Substitution of cellular fatty acids in yeast cells by the antibiotic cerulenin and exogenous fatty acids. Biochim. Biophys. Acta *409*, 267–273. 10.1016/0005-2760(75)90022-3.

28. Zhang, D., and Oliferenko, S. (2013). Remodeling the nuclear membrane during closed mitosis. Curr. Opin. Cell Biol. *25*, 142–148. 10.1016/j.ceb.2012.09.001.

29. Gu, Y., Yam, C., and Oliferenko, S. (2012). Divergence of mitotic strategies in fission yeasts. Nucleus *3*, 37–41. 10.4161/nucl.19514.

30. Makarova, M., and Oliferenko, S. (2016). Mixing and matching nuclear envelope remodeling and spindle assembly strategies in the evolution of mitosis. Curr. Opin. Cell Biol. *41*, 43–50. 10.1016/j.ceb.2016.03.016.

31. Makarova, M., Gu, Y., Chen, J.-S., Beckley, J.R., Gould, K.L., and Oliferenko, S. (2016). Temporal Regulation of Lipin Activity Diverged to Account for Differences in Mitotic Programs. Curr. Biol. *26*, 237–243. 10.1016/j.cub.2015.11.061.

32. Dey, G., Culley, S., Curran, S., Schmidt, U., Henriques, R., Kukulski, W., and Baum, B. (2020). Closed mitosis requires local disassembly of the nuclear envelope. Nature *585*, 119–123. 10.1038/s41586-020-2648-3.

33. Forsburg, S.L., and Rhind, N. (2006). Basic methods for fission yeast. Yeast *23*, 173–183. 10.1002/yea.1347.

34. Schindelin, J., Arganda-Carreras, I., Frise, E., Kaynig, V., Longair, M., Pietzsch, T., Preibisch, S., Rueden, C., Saalfeld, S., Schmid, B., et al. (2012). Fiji: an open-source platform for biological-image analysis. Nat. Methods *9*, 676–682. 10.1038/nmeth.2019.